A Sub-band Divided Ray Tracing Algorithm Using the DPS Subspace in UWB Indoor Scenarios

Mingming Gan[1], Zhinan Xu[1], Markus Hofer[1], Gerhard Steinböck[2], Thomas Zemen[1,3]
[1] FTW Forschungszentrum Telekommunikation Wien, Vienna, Austria
[2] Department of Electronic Systems, Aalborg University, Aalborg, Denmark
[3] AIT Austrian Institute of Technology, Vienna, Austria

***Abstract*—Sub-band divided ray tracing (SDRT) is one technique that has been extensively used to obtain the channel characteristics for ultra-wideband (UWB) radio wave propagation in realistic indoor environments. However, the computational complexity of SDRT scales directly with the number of sub-bands. Although we have proposed a low-complexity SDRT algorithm for one terminal position [1], the computational complexity is still extremely high when involving multiple mobile terminal positions. Moreover, some indoor positioning techniques require for high positioning accuracy data from measurements/simulations with a very fine spatial resolution. To cope with this, we propose an algorithm to reduce the computational complexity of SDRT for multiple mobile terminal positions. The algorithm uses a projection of all propagation paths on a subspace spanned by two-dimensional discrete prolate spheroidal (DPS) sequences at each sub-band. It is important to note that, since the geometrical information of the propagation paths is the same in all sub-bands, the subspace dimension and basis coefficients in frequency dimension do not need to be recalculated at different sub-bands. We justify the simplifications of the proposed method by numerical simulations. Furthermore, we evaluate the effect of antenna characteristics on the proposed algorithm. Our proposed algorithm reduces the computational complexity by more than one order of magnitude for indoor scenarios.**

I. Introduction

Sub-band divided ray tracing (SDRT) applied for ultra-wideband (UWB) systems has been introduced in [2], [3], which has been widely utilized to obtain the channel characteristics in realistic indoor scenarios. It is known that measurement campaigns used for the performance prediction of UWB indoor localization systems are usually time-consuming and tedious to perform. SDRT offers the possibility to predict the radio channel for a certain environment, avoiding the need for measurements when evaluating indoor localization algorithms [4]. However, the computational complexity of SDRT is proportional to the number of the propagation paths and to the number of sub-bands.

The author would like to thank Prof. David J. Edwards and Dr. Gianluigi Tiberi for providing the relevant data for our research work. The research from DEWI project (www.dewi-project.eu) leading to these results has received funding from the ARTEMIS Joint Undertaking under grant agreement no. 621353 and from the Telecommunications Research Center Vienna (FTW). FTW is supported by the Austrian Government and the City of Vienna within the competence center program COMET. This work was also supported by the European FP7 Network of Excellence in Wireless COMmunications NEWCOM# (Grant agreement no. 318306) and in part by the VIRTUOSO cooperative research project, funded by Intel Mobile Communications, Telenor, Anite, Aalborg University, and Innovations Fonden Denmark.

In our previous work, we proposed low-complexity SDRT for a specific terminal position, where ray tracing (RT) only needs to be performed once for a single sub-band [1]. Then the corresponding calculation of propagation paths at other sub-bands can be deduced. When considering multiple mobile terminal positions, this algorithm is still very time-consuming. A parallel ray approximation (PRA) algorithm was proposed in [5] to reduce the computational time. However, the computational time is still proportional to the number of terminal positions.

For band-limited fading processes, it is known that a projection on a subspace spanned by two-dimensional discrete prolate spheroidal (DPS) sequences [6] allows for a substantial complexity reduction of geometry based stochastic channel models [7], [8]. In [9], this insight was applied to obtain a low-complexity DPS subspace based RT algorithm for a wideband communication system in an indoor scenario. We extend the wideband RT in [9] to the UWB case by expanding the DPS sequences to each sub-band. The main contributions of this paper are the following:

- A projection on a subspace spanned by two-dimensional DPS sequences can be used for band-limited fading processes at each sub-band for complexity reduction. Due to the same geometrical information of the propagation paths for all sub-bands, the subspace dimension and basis coefficients in the frequency domain do not need to be recalculated at different sub-bands.
- The accuracy of the proposed algorithm is evaluated by comparing it to low-complexity SDRT without the DPS subspace projection. The numeric simulations include the mean square error (MSE) of channel transfer functions (CTFs) and the root mean square (RMS) delay spread. The effect of antenna characteristics on the proposed algorithm is analyzed.
- Furthermore, the computational time is evaluated. We find that the proposed algorithm reduces the computational time by more than one order of magnitude.

II. SDRT Algorithm

The three-dimensional (3D) RT tool is used in this work to calculate all propagation paths connecting the transmitter (Tx) and the receiver (Rx) based on geometric and electromagnetic computations. The geometric computations determine the propagation paths interacting with the environment. The

electromagnetic computations provide the electric field of the propagation paths in amplitude, phase and polarization according to the considered propagation mechanisms. These propagation mechanisms are line of sight (LOS), reflection, penetration, and diffraction, as well as diffuse scattering. We denote LOS, reflection, penetration, diffraction paths as deterministic paths. The complex dyadic coefficients for reflection and penetration are obtained using Fresnel formulas, while the diffraction coefficients are calculated by the uniform theory of diffraction (UTD) [10]. For the diffuse scattering components, a directive scattering model is implemented in our tool. The scattering lobe related to the scattering tile is assumed to be facing towards the direction of the specular reflection [11]. In addition, a random phase associated with the diffuse scattering path with a uniform distribution is assumed.

The basic idea of SDRT is dividing the entire UWB bandwidth B into I sub-bands with equal bandwidth $B_i \leq 500$ MHz. We index the sub-bands with $i \in \{1, \cdots, I\}$ where I is the total number of the sub-bands. RT is performed at multiple frequencies $f_{\mathrm{c},i}$, which are the center frequencies of each sub-band. It is obvious that the computational complexity of SDRT is proportional to the number of sub-bands. In [5], a first simplification has been proposed by performing the geometric computation once at the beginning of the procedure, while the electromagnetic calculation are performed at each individual frequency $f_{\mathrm{c},i}$. We proposed a low-complexity SDRT algorithm in [1], where both the geometric computation and the electromagnetic computation need to be performed only once for all sub-bands. The corresponding calculation of propagation paths at other sub-bands can be derived based on the results at one sub-band. Details can be found in [1].

For a static Tx and multiple Rx positions, the CTF depends on the Rx positions $\mathbf{u}_n$. We are interested in the case that $\mathbf{u}_n = \mathbf{u}_0 + \mathbf{d}_{\mathrm{S}} n$, where $n \in \{0, \cdots, N-1\}$ is the discrete Rx position index and N is the number of samples in the space domain, $\mathbf{u}_0$ is the initial Rx position, and $\mathbf{d}_{\mathrm{S}}$ is the spatial resolution vector. The CTF based on low-complexity SDRT at one sub-band can be obtained as

$$\begin{aligned} H^i_{\mathrm{SDRT}}[q_i, \mathbf{u}_n] &= H^i_{\mathrm{SDRT}}(q_i f_{\mathrm{S}}, \mathbf{u}_0 + \mathbf{d}_{\mathrm{S}} n) \\ &= \sum_{l=1}^{L} \eta_l[f_{\mathrm{c},i}, \mathbf{u}_n] e^{-j2\pi q_i \theta_l[\mathbf{u}_n]}, \end{aligned} \tag{1}$$

where f_{S} denotes the width of a frequency bin, $l \in \{1, \cdots, L\}$ is the index of the propagation paths, L is the total number of propagation paths, $\theta_l[\mathbf{u}_n] = \tau_l[\mathbf{u}_n] f_{\mathrm{S}}$ is the normalized delay of the $l-$th path with τ_l denoting the excess delay of the l-th path, where the delay of the first arriving path is defined as $\tau_1 = 0\,\mathrm{s}$, $\eta_l[f_{\mathrm{c},i}, \mathbf{u}_n]$ is the complex electric field of the l-th path at the center frequency $f_{\mathrm{c},i}$ of the i-th sub-band, $q_i \in \{-\lfloor \frac{Q_i}{2} \rfloor, \ldots, \lfloor \frac{Q_i}{2} \rfloor - 1\}$ is the discrete frequency index vector at the i-th sub-band, Q_i is the number of samples in the frequency domain at the i-th sub-band, and $\lfloor \cdot \rfloor$ indicates the floor function. Both η_l and τ_l depend on the Rx positions $\mathbf{u}_n$. Finally, the relevant H_{SDRT} in the entire frequency range can be obtained by combing all CTFs H^i_{SDRT} at different sub-bands as

$$\begin{aligned} H_{\mathrm{SDRT}}[q, \mathbf{u}_n] = \big[& H^1_{\mathrm{SDRT}}[q_1, \mathbf{u}_n]^{\mathrm{T}} \\ & H^2_{\mathrm{SDRT}}[q_2, \mathbf{u}_n]^{\mathrm{T}} \cdots \; H^I_{\mathrm{SDRT}}[q_I, \mathbf{u}_n]^{\mathrm{T}} \big]^{\mathrm{T}}, \end{aligned} \tag{2}$$

where $[\cdot]^{\mathrm{T}}$ denotes the transpose function.

III. Computational Complexity Reduction

In the following we present our method for reducing the computational complexity by means of a projection on a subspace spanned by DPS sequences. To reduce the computational complexity of low-complexity SDRT for multiple Rx positions, we propose a low-complexity DPS subspace based RT algorithm. The prerequisite of the proposed algorithm is to fulfill the same conditions as the PRA algorithm. Therefore, we introduce first the PRA algorithm and thereafter the extensions with the DPS sequences. Note that RT needs to be performed only once at one sub-band at the initial Rx position $\mathbf{u}_0$ for these two algorithms.

A. PRA Algorithm Based on Low-Complexity SDRT

PRA is an efficient RT algorithm for modeling UWB indoor propagation channels at multiple terminal positions [5]. The basic concept is that the gain coefficients of propagation paths reaching the nearby targets are assumed to have the same magnitude but different phases. This approximation is valid when the following farfield conditions are fulfilled [5]:

$$|\mathbf{u}_{\mathrm{Tx}} - \mathbf{u}_0| \gg \lambda_{\mathrm{l}}, \tag{3}$$

$$|\mathbf{u}_{\mathrm{Tx}} - \mathbf{u}_0| \gg |\mathbf{u}_n - \mathbf{u}_0| = |\mathbf{d}_{0,n}|, \tag{4}$$

where λ_{l} is the wavelength at the lowest center frequency, $\mathbf{u}_{\mathrm{Tx}}$ is the Tx position coordinate, and $\mathbf{d}_{0,n}$ is the vector pointing to the Rx position $\mathbf{u}_n$ from the initial Rx position $\mathbf{u}_0$. The CTF at the Rx position $\mathbf{u}_n$, relying on the results of the initial Rx position $\mathbf{u}_0$, at the i-th sub-band is approximated as

$$H^i_{\mathrm{PRA}}[q_i, \mathbf{u}_n] \approx \sum_{l=1}^{L} \eta_l[f_{\mathrm{c},i}, \mathbf{u}_0] e^{-j2\pi q_i \theta_l[\mathbf{u}_0]} e^{j\frac{2\pi \mathbf{d}_{0,n} \cdot \mathbf{v}_l}{\lambda_{\mathrm{c},i}}}, \tag{5}$$

$\lambda_{\mathrm{c},i}$ is the wavelength corresponding to $f_{\mathrm{c},i}$, and $\mathbf{v}_l$ is the unit vector of the l-th path reaching $\mathbf{u}_0$. Furthermore, the relevant H_{PRA} in the entire frequency range can be obtained in the same manner as in (2).

B. DPS Subspace Algorithm Based on Low-Complexity SDRT

We exploit the band-limited property of the CTF by projecting each path $l \in \{1, \ldots, L\}$ to a subspace spanned by two-dimensional DPS sequences [6]. The two-dimensions refer to the frequency and space dimension. The two key parameters for the setup of the i-th sub-band are

- the maximum normalized excess delay $\theta_{\mathrm{Dmax},i} = \tau_{\mathrm{max},i} f_{\mathrm{S}}$, where $\tau_{\mathrm{max},i}$ is the maximum excess delay among all paths at the initial Rx position $\mathbf{u}_0$ for the i-th sub-band, and
- the normalized minimum and maximum direction of arrival (DoA) $\xi_{\mathrm{Dmin},i} = \cos(\psi_{\mathrm{min},i}) \frac{\|\mathbf{d}_{\mathrm{S}}\|}{\lambda_{\mathrm{c},i}}$ and $\xi_{\mathrm{Dmax},i} = \cos(\psi_{\mathrm{max},i}) \frac{\|\mathbf{d}_{\mathrm{S}}\|}{\lambda_{\mathrm{c},i}}$, where $\|\mathbf{d}_{\mathrm{S}}\|$ is the distance between

antenna positions, $\|\cdot\|$ denotes Euclidean norm, the DoA ψ is defined as the angle between $\mathbf{d}_{0,n}$ and $\mathbf{v}_l$, $\psi_{\min,i}$ and $\psi_{\max,i}$ are the minimum and maximum DoAs among all paths at the initial Rx position $\mathbf{u}_0$ for the i-th sub-band.

As mentioned previously the geometric computation of propagation paths is the same for all sub-bands, so $\tau_{\max,i}$, $\psi_{\min,i}$ and $\psi_{\max,i}$ are independent of the sub-band. Thus, $\theta_{\mathrm{Dmax},i}$ is also independent of the sub-band. We drop the index i from $\theta_{\mathrm{Dmax},i}$ and write θ_{Dmax} in the rest of the paper. However, $\xi_{\mathrm{Dmin},i}$ and $\xi_{\mathrm{Dmax},i}$ are related to the sub-band because of their dependency on $\lambda_{\mathrm{c},i}$. The band-limited region at the i-th sub-band is defined by the Cartesian product as [7]

$$\begin{aligned}\mathcal{W}_i =& W_{\mathrm{f}} \times W_{\mathrm{d}i} = \\ & [0, \theta_{\mathrm{Dmax}}] \times [\frac{\xi_{\mathrm{Dmin},i} + \xi_{\mathrm{Dmax},i}}{2}, \frac{\xi_{\mathrm{Dmax},i} - \xi_{\mathrm{Dmin},i}}{2}].\end{aligned} \tag{6}$$

The relevant index set is denoted by

$$\mathcal{I}_i = I_{\mathrm{f}i} \times I_{\mathrm{d}} = \{-\lfloor\frac{Q_i}{2}\rfloor, \ldots, \lfloor\frac{Q_i}{2}\rfloor - 1\} \times \{0, \ldots, N-1\}. \tag{7}$$

The approximate DPS subspace representation $H_{\mathrm{DPS}}^{(D_i)}$ with the subspace dimension D_i for the i-th sub-band can be expressed as

$$H_{\mathrm{DPS}}^{(D_i)}[q_i, \mathbf{u}_n] \approx \boldsymbol{V_i}\tilde{\boldsymbol{\alpha}}_i, \tag{8}$$

where the two-dimensional DPS basis vector at the i-th sub-band is

$$\boldsymbol{V_i} = \boldsymbol{V_i}(\mathcal{W}_i, \mathcal{I}_i) = \boldsymbol{V_i}(W_{\mathrm{f}}, I_{\mathrm{f}i}) \diamond \boldsymbol{V_i}(W_{\mathrm{d}i}, I_{\mathrm{d}}). \tag{9}$$

The operator $\diamond$ is the Tracy-Singh product of column-wise partitioned matrices [12] and $\tilde{\boldsymbol{\alpha}}_i$ are the approximate basis coefficients. It can be observed that the basis vectors $\boldsymbol{V_i}(W_{\mathrm{f}}, I_{\mathrm{f}i})$ and $\boldsymbol{V_i}(W_{\mathrm{d}i}, I_{\mathrm{d}})$ change along different sub-bands. The approximate basis coefficients at the i-th sub-band can be expressed by a Kronecker product

$$\begin{aligned}\tilde{\boldsymbol{\alpha}}_i = \sum_{l=1}^{L} \eta_l[f_{\mathrm{c},i}, \mathbf{u}_0] & \underbrace{(\boldsymbol{V_i}(W_{\mathrm{f}}, I_{\mathrm{f}i})\boldsymbol{\chi}_{\mathrm{f}i}(\theta_l))}_{\gamma^{\mathrm{f}}_{l,i} :\approx \tilde{\gamma}^{\mathrm{f}}_{l,i}(\tau_l; W_{\mathrm{f}}, I_{\mathrm{f}i})} \\ & \otimes \underbrace{(\boldsymbol{V_i}(W_{\mathrm{d}i}, I_{\mathrm{d}})\boldsymbol{\chi}_{\mathrm{d}i}(\xi_{l,i}))}_{\gamma^{\mathrm{d}}_{l,i} :\approx \tilde{\gamma}^{\mathrm{d}}_{l,i}(\psi_l; W_{\mathrm{d}i}, I_{\mathrm{d}})},\end{aligned} \tag{10}$$

where ψ_l is the DoA of the l-th path, while $\xi_{l,i}$ is the normalized DoA at the i-th sub-band, and

$$\boldsymbol{\chi}_{\mathrm{f}i}(\theta_l) = [\vartheta_{\mathrm{f}}^{(-\lfloor\frac{Q_i}{2}\rfloor)}, \vartheta_{\mathrm{f}}^{(-\lfloor\frac{Q_i}{2}\rfloor+1)}, \ldots, \vartheta_{\mathrm{f}}^{(\lfloor\frac{Q_i}{2}\rfloor-1)}]^{\mathrm{T}} \tag{11}$$

and

$$\boldsymbol{\chi}_{\mathrm{d}i}(\xi_{l,i}) = [\vartheta_{\mathrm{d}i}^{0}, \vartheta_{\mathrm{d}i}^{1}, \ldots, \vartheta_{\mathrm{d}i}^{(N-1)}]^{\mathrm{T}} \tag{12}$$

are the complex exponential functions, in which $\vartheta_{\mathrm{f}} = e^{-j2\pi\theta_l}$ and $\vartheta_{\mathrm{d}i} = e^{j2\pi\xi_{l,i}}$, respectively. Then the approximated projections of the complex exponential functions on the DPS basis vectors $\tilde{\gamma}^{\mathrm{f}}_{l,i}(\tau_l; W_{\mathrm{f}}, I_{\mathrm{f}i})$ and $\tilde{\gamma}^{\mathrm{d}}_{l,i}(\psi_l; W_{\mathrm{d}i}, I_{\mathrm{d}})$ can be used to simplify the calculation of the complex exponential functions by the scaled and shifted approximated DPS wave functions [7]. It can be seen that the approximated projection $\tilde{\gamma}^{\mathrm{f}}_{l,i}(\tau_l; W_{\mathrm{f}}, I_{\mathrm{f}i})$ and $\tilde{\gamma}^{\mathrm{d}}_{l,i}(\psi_l; W_{\mathrm{d}i}, I_{\mathrm{d}})$ are related to the sub-band. However, if we have the same number of sampled frequencies Q_i for all sub-bands, only the approximated projection $\tilde{\gamma}^{\mathrm{d}}_{l,i}(\psi_l; W_{\mathrm{d}i}, I_{\mathrm{d}})$ in space is related to the sub-band. Finally, the relevant $H_{\mathrm{DPS}}^{(D)}[q, \mathbf{u}_n]$ in the entire frequency range can be obtained

$$\begin{aligned}H_{\mathrm{DPS}}[q, \mathbf{u}_n] = \big[&H_{\mathrm{DPS}}^{(D_1)}[q_1, \mathbf{u}_n]^{\mathrm{T}} \\ & H_{\mathrm{DPS}}^{(D_2)}[q_2, \mathbf{u}_n]^{\mathrm{T}} \cdots \; H_{\mathrm{DPS}}^{(D_I)}[q_I, \mathbf{u}_n]^{\mathrm{T}}\big]^{\mathrm{T}}.\end{aligned} \tag{13}$$

IV. Simulation Procedure

In order to show the performance of the proposed algorithm, a typical indoor scenario is generated according to the measurements description in [5]. Moreover, we consider two antennas with different radiation patterns in the evaluation: i) discone antennas [13] and ii) omnidirectional antennas at both Tx and Rx sides, respectively.

A. Simulation Configuration

A 3-D view of the scenario is shown in Fig.1, whose dimensions are $5.7\,\mathrm{m} \times 5\,\mathrm{m} \times 2.6\,\mathrm{m}$. It consists of a concrete floor and ceiling, concrete walls, a wooden door, glass windows, as well as metallic and wooden furniture. Different materials are sketched with different colors in Fig.1. The dielectric parameters can be found in [5], and we treat the metallic cabinet as a perfect electric conductor. The location of the Tx antenna is fixed, whose coordinate is $\mathbf{u}_{\mathrm{Tx}} = [0.775\ 2.755\ 1.35]^{\mathrm{T}}\,\mathrm{m}$. The Rx antenna is placed linearly at $N = 200$ positions seen from the lower right corner of Fig. 1. The initial coordinate of the Rx is $\mathbf{u}_0 = [3.08\ 2.73\ 1.35]^{\mathrm{T}}\,\mathrm{m}$. We consider a fixed Rx antenna height, so that the spatial resolution vector is set as $\mathbf{d}_{\mathrm{S}} = [\frac{\sqrt{2}}{2}\ \frac{\sqrt{2}}{2}\ 0]^{\mathrm{T}}\,\mathrm{mm}$, resulting in Rx antenna separation of $\|\mathbf{d}_{\mathrm{S}}\| = 1\,\mathrm{mm}$. A close-up view of the Rx positions is included in Fig.1. A few exemplary propagation paths are visualized in Fig.1 for the Rx position $\mathbf{u}_0$. In the simulation, we consider the propagation mechanisms including LOS, up to the fourth order reflections, penetration, single order diffraction and diffuse scattering. Note that penetration is embedded in all other mechanisms.

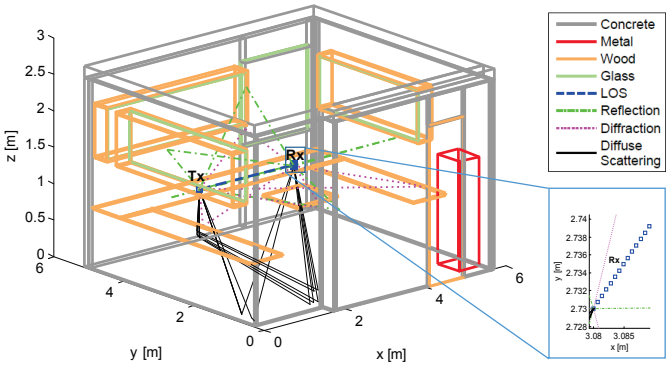

Fig. 1. 3-D view of the measurement environment including a close-up view of Rx positions.

The frequency range is from $3.1\,\mathrm{GHz}$ to $10.6\,\mathrm{GHz}$ with a frequency resolution of $f_{\mathrm{S}} = 4.6875\,\mathrm{MHz}$. We divide the

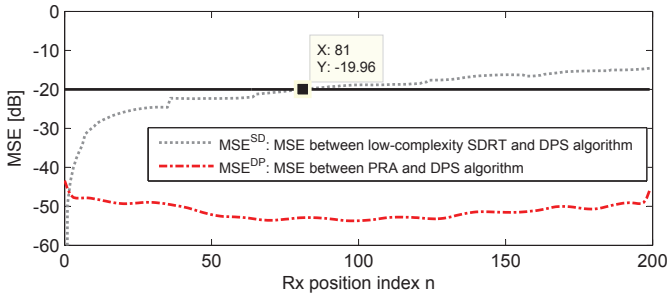

(a) Discone antenna

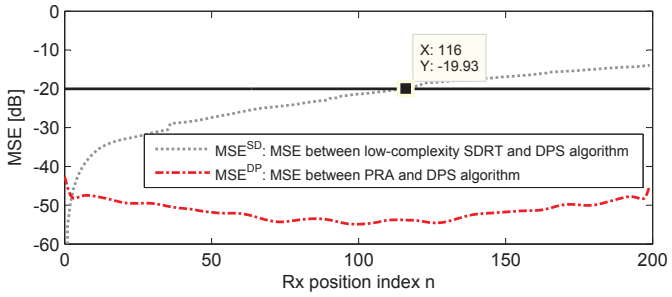

(b) Omnidirectional antenna

Fig. 2. MSE of CTFs based on three algorithms, which only consider the deterministic paths, at the same Rx positions.

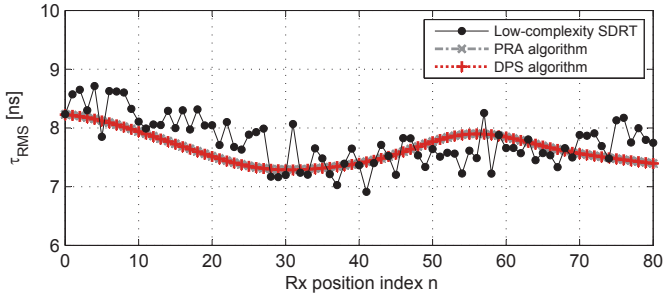

(a) Discone antenna

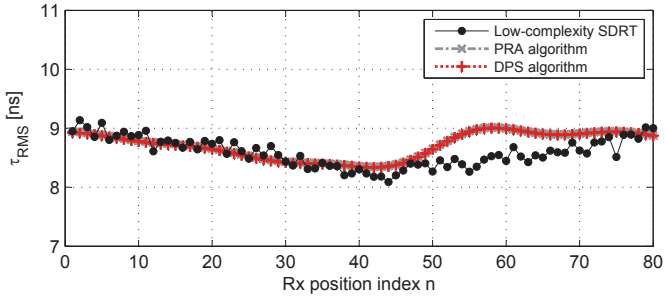

(b) Omnidirectional antenna

Fig. 3. Comparison of RMS delay spread τ_{RMS} based on three algorithms at the same Rx positions.

entire bandwidth of 7.5 GHz into $I = 16$ sub-bands with bandwidth $B_i = 468.75$ MHz. Note that $Q_i = 100$ for all sub-bands. Thus, the corresponding calculation of the subspace dimension $\boldsymbol{V_i}(W_{\mathrm{f}}, I_{\mathrm{f}i})$ and its relevant basis coefficients $\tilde{\gamma}^{\mathrm{f}}_{l,i}(\tau_l; W_{\mathrm{f}}, I_{\mathrm{f}i})$ in frequency need to be performed only once. In the following analysis, the low-complexity SDRT algorithm is served as a reference [1]. There are $L = 60945$ propagation paths obtained based on low-complexity SDRT at the first sub-band B_1 of the initial position $\mathbf{u}_0$.

B. MSE Comparison

The MSE of the CTFs between low-complexity SDRT and the DPS subspace algorithm can be calculated as (14)

$$\mathrm{MSE}[\mathbf{u}_n] = \frac{\sum_q |H_{\mathrm{SDRT}}[q, \mathbf{u}_n] - H_{\mathrm{DPS}}[q, \mathbf{u}_n]|^2}{\sum_q |H_{\mathrm{SDRT}}[q, \mathbf{u}_n]|^2}. \qquad (14)$$

The MSE between the remaining algorithms can be calculated in the same way. Note that the low-complexity SDRT assumes that the random phases of diffuse scattering paths are drawn independently for each Rx position, while the PRA and DPS algorithms are initialized the relevant phases from Rx position $\mathbf{u}_0$. Thus, in order to avoid the influences from the random phases of diffuse scattering paths, we only consider the deterministic paths to obtain the associated $\mathrm{MSE}[\mathbf{u}_n]$ results. The relevant results are shown in Fig. 2, which includes two different antenna cases. It can be noticed that the MSE values between the PRA and DPS algorithms are always smaller than -45 dB for both antenna cases. This confirms that the approximation of the DPS subspace algorithm is as good as the PRA algorithm.

We can observe a jump in the MSE values at the Rx position $\mathbf{u}_{36}$ for both antenna cases. We find at the Rx position $\mathbf{u}_{36}$ in comparison to the Rx positions $\mathbf{u}_{\{n\leq 35\}}$ two additional deterministic components in the low complexity SDRT algorithm. These components are obviously not included in the PRA and DPS algorithms, which leads to the jump in the MSE.

We set the acceptable error threshold to $\mathrm{MSE}_{\mathrm{thr}} = -20$ dB, which indicates how accurate the proposed DPS algorithm is expected to be. With both antenna cases, the MSE between the RT and DPS subspace algorithm increases steadily along all Rx positions. For the discone antenna case, the MSE keeps smaller than -20 dB until the Rx position $\mathbf{u}_{80}$. While for the omnidirectional antenna case, the MSE starts to exceed -20 dB from the Rx position $\mathbf{u}_{116}$. It can be concluded that the antenna radiation pattern can influence the accuracy of the proposed DPS algorithm. In order to make the relevant results comparable, the considered maximum number of Rx positions is set to $N = 81$ for the remainder of this paper, which is equal to 8 cm[1].

C. RMS Delay Spread Comparison

In Fig. 3, the RMS delay spreads τ_{RMS} are shown for the three SDRT implementations and the two antenna configurations. It can be observed from Fig. 3 that the τ_{RMS} values based on low-complexity SDRT fluctuate. The τ_{RMS} values do not fluctuate for the PRA and DPS cases, but evolve rather smoothly. This is related to the random phases of the diffuse scattering paths, please refer to IV-B for the detailed explaination. It also can be seen that the τ_{RMS} values for the PRA and DPS algorithm are practically identical. For

[1]If the environment is larger, resulting in interactions to be further away and the plane wave assumptions to be better fulfilled, the MSE would increase slower and the maximum possible 'N' under the threshold would be larger.

TABLE I
COMPUTATIONAL TIMES

Algorithms	SDRT [h]	PRA [h]	DPS [h]
Computational time	6.78	0.078	0.012

the discone antenna case, the τ_{RMS} differences between low-complexity SDRT and the DPS algorithm is always smaller than 1 ns along all Rx positions, while for the omnidirectional antenna case, it is always smaller than 0.5 ns along all Rx positions. This is mainly caused by the antenna elevation pattern. It can be concluded that the antenna radiation pattern influences the RMS delay spread as well, however to a smaller degree.

D. Computational Time Comparison

The computational time comparison (2.4 GHz Intel Core i7 CPU with 8 GB RAM) based on the three considered low-complexity algorithms are presented in Table I. The common simulation time of 0.086 h of RT for all three algorithms performed at one sub-band at the initial Rx position $\mathbf{u}_0$ is not included. Note that the computational times are the same for both antenna configurations. Compared to low-complexity SDRT, the computation time can be reduced by a factor of $(6.78 + 0.086)/(0.012 + 0.086) = 70.06$ when using the DPS algorithm. While compared to the PRA algorithm, without considering the simulation time of RT performed at one sub-band at the initial Rx position $\mathbf{u}_0$, the corresponding reduction factor is about 6.5.

The essential subspace dimensions in frequency and space are the same for both antennas, respectively. The essential subspace dimension in frequency is $D_{\text{f}} = 74$ for all sub-bands, while in space $D_{\text{d}}(i)$ varies for different sub-bands. $D_{\text{d}}(i)$ is shown in Fig. 4. It is evident that the subspace dimension in frequency is always smaller than the number of frequency samples in each sub-band. In addition, the dimension in space at different sub-bands is always smaller than the number of Rx positions. Therefore, we reduce the computational time with the DPS subspace algorithm.

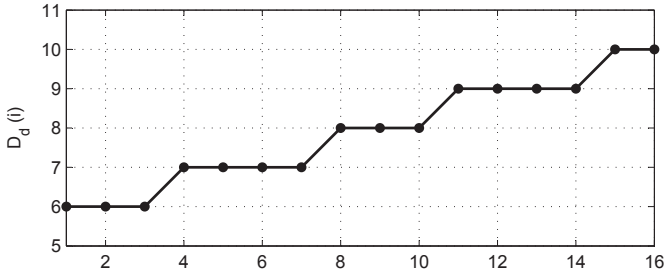

Fig. 4. Subspace dimension $D_{\text{d}}(i)$ in space.

V. CONCLUSION

We presented a SDRT algorithm using a projection on DPS subspaces to reduce the computational complexity for multiple Rx positions in UWB indoor scenarios. The proposed DPS subspace algorithm requires RT results only at one sub-band at the initial Rx position in order to obtain CTFs for the remaining Rx positions. Because the geometrical information of the propagation paths is the same for all sub-bands, the subspace dimension and the basis coefficients in frequency domain need to be calculated only once for all sub-bands. Moreover, we evaluated the accuracy of the proposed algorithm, opposed to low-complexity SDRT. The accuracy evaluation includes the MSE of CTFs and the RMS delay spread. In addition, we considered the effect of antenna characteristics on the proposed algorithm. We found that the antenna radiation pattern influences the MSE of CTFs and the RMS delay spread. Furthermore, the computational time of these algorithms were analyzed. The proposed DPS subspace algorithm reduces the computational time by more than one order of magnitude compared to low-complexity SDRT.

REFERENCES

[1] M. Gan, P. Meissner, F. Mani, E. Leitinger, M. Frohle, C. Oestges, K. Witrisal, and T. Zemen, "Low-complexity sub-band divided ray tracing for UWB indoor channel," in *Wireless Communications and Networking Conference (WCNC), 2014 IEEE*, April 2014, pp. 305–310.

[2] H. Sugahara, Y. Watanabe, T. Ono, K. Okanoue, and S. Yarnazaki, "Development and experimental evaluations of "RS-2000" - a propagation simulator for UWB systems," in *Ultra Wideband Systems, Joint with Conference on Ultrawideband Systems and Technologies. Joint UWBST IWUWBS. 2004 International Workshop on*, May 2004, pp. 76 – 80.

[3] J. Jemai, P. Eggers, G. Pedersen, and T. Kürner, "On the applicability of deterministic modelling to indoor UWB channels," in *Proceedings of the 3rd Workshop on Positioning, Navigation and Communication (WPNC'06)*, 2006.

[4] P. Meissner, M. Gan, F. Mani, E. Leitinger, M. Fröhle, C. Oestges, T. Zemen, and K. Witrisal, "On the use of ray tracing for performance prediction of uwb indoor localization systems," in *Communications Workshops (ICC), 2013 IEEE International Conference on*, June 2013, pp. 68–73.

[5] G. Tiberi, S. Bertini, W. Malik, A. Monorchio, D. Edwards, and G. Manara, "Analysis of realistic ultrawideband indoor communication channels by using an efficient ray-tracing based method," *Antennas and Propagation, IEEE Transactions on*, vol. 57, no. 3, pp. 777 – 785, Mar. 2009.

[6] D. Slepian, "Prolate spheroidal wave functions, Fourier analysis, and uncertainty - V:the discrete case," *The Bell System Technical Journal*, vol. 57, no. 5, pp. 1371 – 1430, 1978.

[7] F. Kaltenberger, T. Zemen, and C. W. Ueberhuber, "Low-complexity geometry-based MIMO channel simulation," *EURASIP Jounal in Advanced Signal Processing*, vol. 2007, 2007.

[8] N. Czink, F. Kaltenberger, Y. Zhou, L. Bernado, T. Zemen, and X. Yin, "Low-complexity geometry-based modeling of diffuse scattering," in *Antennas and Propagation (EuCAP), 2010 Proceedings of the Fourth European Conference on*, April 2010, pp. 1 – 4.

[9] M. Gan, F. Mani, F. Kaltenberger, C. Oestges, and T. Zemen, "A ray tracing algorithm using the discrete prolate spheroidal subspace," in *Communications (ICC), 2013 IEEE International Conference on*, June 2013, pp. 5710–5714.

[10] C. Oestges, B. Clerckx, L. Raynaud, and D. Vanhoenacker-Janvier, "Deterministic channel modeling and performance simulation of microcellular wide-band communication systems," *Vehicular Technology, IEEE Transactions on*, vol. 51, no. 6, pp. 1422 – 1430, Nov. 2002.

[11] V. Degli-Esposti, F. Fuschini, E. M. Vitucci, and G. Falciasecca, "Measurement and modelling of scattering from buildings," *Antennas and Propagation, IEEE Transactions on*, vol. 55, no. 1, pp. 143 – 153, Jan. 2007.

[12] T. Zemen and A. Molisch, "Adaptive reduced-rank estimation of non-stationary time-variant channels using subspace selection," *Vehicular Technology, IEEE Transactions on*, vol. 61, no. 9, pp. 4042 – 4056, Nov. 2012.

[13] W. Malik, D. Edwards, and C. Stevens, "Angular-spectral antenna effects in ultra-wideband communications links," *Communications, IEEE Proceedings on*, vol. 153, no. 1, pp. 99–106, Feb. 2006.